Fine Chemical Engineering
http://ojs.wiserpub.com/index.php/FCE/

Research Article

NH_2-modification Copper Metal-organic Framework as a Sunlight Photocatalyst for the Removal of Organic Dyes from Aqueous Solution

Qi Wang, Qianqian Xu, Jiawei Zhang, Long Fang, Kai Xia, Deshuai Sun*

College of Chemistry & Chemical Engineering, Qingdao University, Qingdao 266071, China
E-mail: luckysds@163.com

Received: 12 September 2023; **Revised:** 7 November 2023; **Accepted:** 13 November 2023

Abstract: Dyes present in wastewater pose a threat to aquatic organisms and cannot be effectively eliminated by conventional biochemical treatment methods. As an alternative, the photocatalytic decolorization of dyes has emerged as a cost-effective and environmentally friendly approach. Two 1,3,5-benzenetricarboxylate (BTC)-based metal-organic frameworks (MOFs), CuBTC and CuBTC-NH_2, were synthesized and used for the removal of two anionic dyes, namely Reactive Blue 171 and Acid Blue 1, from wastewater under sunlight irradiation. The structural and morphological characteristics of the MOFs were identified using Fourier transform infrared spectroscopy, X-ray diffraction, and scanning electron microscopy. Compared to CuBTC, CuBTC-NH_2 exhibited excellent photocatalytic activity. The successful degradation of 90% of the dyes was observed within 24 h of sunlight exposure using CuBTC-NH_2, while only 70% degradation was achieved with CuBTC. The weak basic nature of the dye wastewater (pH 8-10) was found to facilitate the degradation process. CuBTC-NH_2 was not only efficient in the removal of dyes but could also be recycled and reused for at least five cycles. In the process of photocatalytic degradation, the diazo bond of dyes in ortho-position to the amino substitution on the aromatic ring was attacked first. These results provide insights into the design of MOF catalysts for dye removal under visible-light irradiation.

Keywords: CuBTC-NH_2 metal-organic framework, anionic dyes, photocatalytic degradation, sunlight irradiation

1. Introduction

Textile printing and dyeing processes are characterized by high water consumption, resulting in the generation of large volumes of wastewater. Dyes in wastewater are toxic to aquatic organisms and also contribute to the high color intensity of the water.[1,2] Discharging such wastewater into the aquatic environment can restrict the penetration of sunlight through the water, thus affecting the photosynthesis of aquatic plants.[3] Consequently, dyes must be removed from these colored effluents before they are discharged into the environment to reduce the harmful effects of dyes on the ecosystem.[4,5]

Various techniques for wastewater treatment, such as adsorption,[6,7] biological treatment, and chemical oxidation,[8] are currently employed to remove dye pollutants from aqueous solutions. However, no single process is capable of providing adequate treatment for these effluents. Because many dyes are resistant to biological degradation, the combination of biological oxidation and adsorption is the conventional technology to remove organic dyes from wastewater,[9] which is limited by high costs and the occurrence of secondary pollution. In the last decades, advanced

DOI: https://doi.org/10.37256/fce.5120243652

oxidation processes based on photocatalysis have attracted increasing attention in the field of wastewater treatment due to their strong oxidizing ability and highly efficient degradation of organic compounds. Dyes can be converted into organic substances with low molecular weight or into inorganic matter without toxic properties through the irradiation of ultraviolet (UV) or visible light in the presence of a suitable catalyst.[10,11] Titanium dioxide (TiO_2) was the common photocatalyst used in dye degradation processes under UV irradiation. However, since the catalytic degradation under UV light utilizes only four percent of the solar spectrum, a relatively low utilization rate of sunlight is achieved in such TiO_2-catalyzed degradations.[12] In addition, the quantum efficiency of TiO_2 is low because of its large bandgap.[13]

Due to their large specific surface area and high porosity, metal-organic framework (MOF) materials are widely used in adsorption and heterogeneous catalysis.[14] In the MOF family, MOF-5 with a structure of 1,4-terephthalate-connected Zn_4O units was first used as photocatalyst for phenol degradation[15,16] with photosensitivity over a wide wavelength range. As expected, Ti-based MOFs demonstrated photocatalytic activity.[17] Fe-based MOFs (Fe-MIL-101, Fe-MIL-100, and Fe-MIL-53) were also reported to possess visible-light harvesting ability.[18] Fe-MIL-101 was found to achieve 96.6% tetracycline removal[19] and 87.1% Rhodamine B removal under visible-light irradiation.[18] To improve the visible-light response, the organic linkers in MOFs should be carefully selected. The amine group in the organic ligand significantly enhanced the visible-light-responsive properties of MOF materials. Fu et al. showed that NH_2-MIL-125(Ti) was an excellent photosensitive catalyst for CO_2 reduction compared with MIL-125(Ti).[17] MIL-68(In)-NH_2 performed as an efficient visible-light-driven photocatalyst with considerable activity and stability for the reduction of Cr(VI).[20] Porous NH_2-MIL-101(Fe) showed both excellent performance and stability in the photodegradation of azo dyes.[21]

In this work, Cu-based MOFs were selected as potential catalysts because they are environmentally friendly, inexpensive, and easy to recover.[22] To enhance the visible-light-responsive properties, the amino group was introduced into MOFs as a secondary group for functionalization.[23] CuBTC-NH_2 was fabricated by post-treatment to increase the sensibility to visible light. The material was characterized by Fourier transform infrared (FT-IR) spectroscopy, X-ray diffraction (XRD), and nitrogen adsorption-desorption analysis. CuBTC-NH_2 was used to catalyze the degradation of two organic dyes (Acid Black 1 and Reactive Blue 171) under exposure to sunlight. The possible mechanistic pathways for dye degradation were also suggested. It is expected that this work can provide new insights into methods to tune photocatalysts for the degradation of organic dyes.

2. Experimental

2.1 *Chemicals*

Table 1. Chemical properties of dyes

Property	AB1	RB171
Molecular weight[a]	570.5	1281.0
Width(nm)[a]	2.171	31.986
Depth(nm)	0.619	14.086
Thickness(nm)	0.475	6.207
λ_{max}(nm)	615	600
Number of ionizable group	2	6

[a] the stereochemical structures were optimized calculated by ChemSketch 12.0

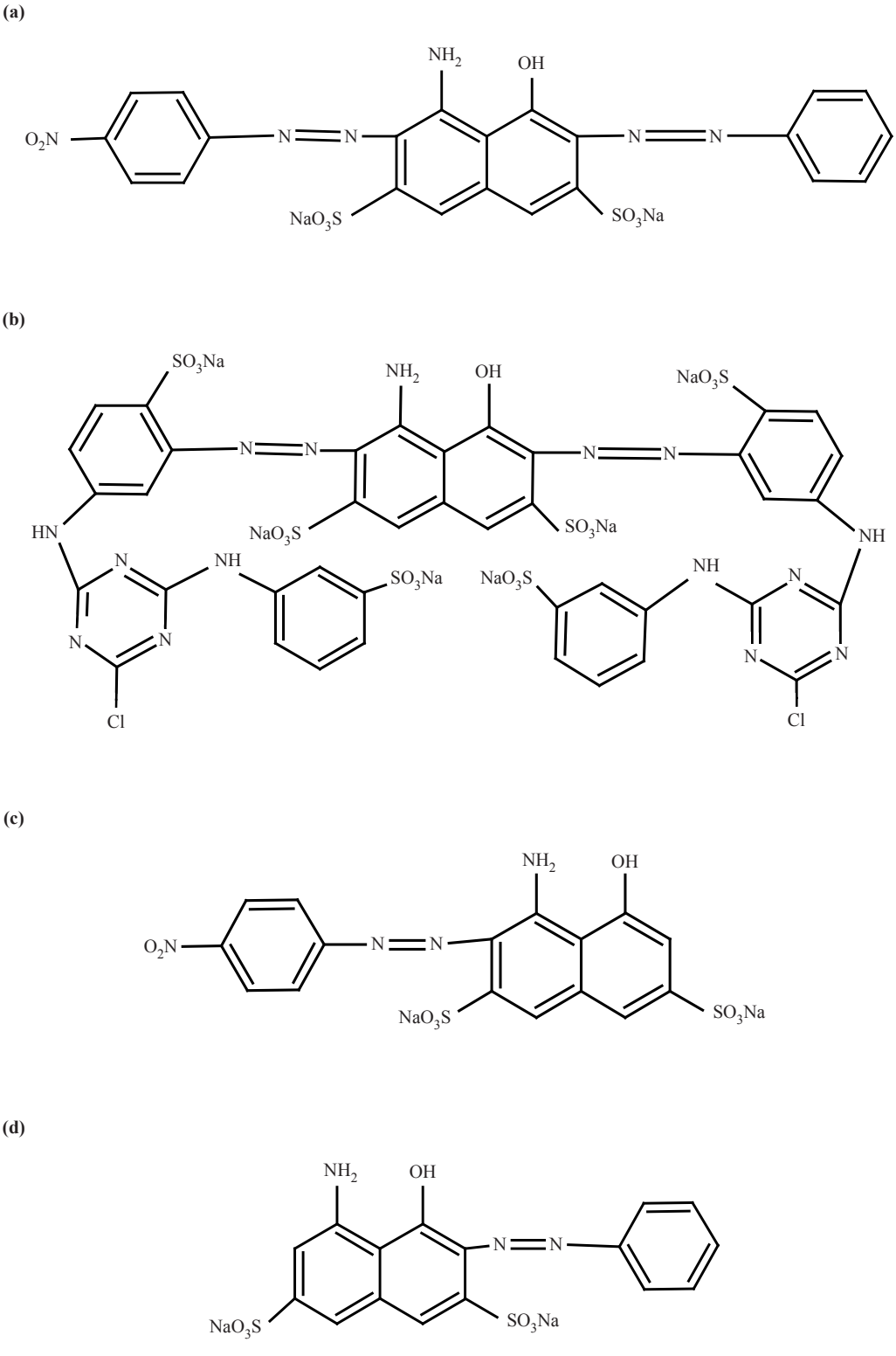

Figure 1. Chemical structure of dyes of (a)Acid Black 1, (b) Reactive Blue 171 and dye intermediates of (c) AB1-L and (d) AB1-R

The chemicals $Cu(NO_3)_2 \cdot 3H_2O$, ethanol, and ethylene diamine were purchased from Sinopharm Chemical Reagent

Co., Ltd. 1,3,5-Benzenetricarboxylic acid (1,3,5-H_3BTC) was provided by Macklin Biochemical Technology Co., Ltd. All chemicals were analytical grade and used without further purification. The organic dyes (Figure 1) were Acid Black 1 (AB1) and Reactive Blue 171 (RB171), which were supplied by Decai Pigment & Chemical Engineering Co., Ltd. (China). Table 1 lists the basic chemical properties. To analyze the degradation process, two dye intermediates related to AB1 (AB1-L and AB1-R) were used (Figure 1).

2.2 *Catalyst preparation*

CuBTC was prepared by an improved solvothermal method.[24] To initiate the synthesis, a solution of 0.875 g $Cu(NO_3)_2 \cdot 3H_2O$ in deionized water (12 mL) was mixed with a ligand solution of 0.42 g 1,3,5-H_3BTC in ethanol (12 mL). The resulting mixture was stirred and sonicated for 10 min at room temperature until it became clear. Then, the clear solution was transferred to a polytetrafluoroethylene reactor and heated at 120 °C for 12 h. After the reaction, the resulting solid was separated by centrifugation and then washed with a mixture of deionized water and ethanol (1:1). The bluish violet powder was dried at 100 °C for 5 h.

CuBTC-NH_2 was obtained through a post-modification of CuBTC.[25] CuBTC was dried at 105 °C for 24 h to remove all water present in micropores. The material was added to a toluene solution (30 mL) of ethylene diamine (0.05 mL). The mixture reacted at 60 °C for 5 h. After the reaction, the blue microcrystals were separated by centrifugation, and the blue powder was washed with ethanol and then dried at 100 °C for 5 h. When the quantity of ethylene diamine was doubled, the obtained MOF material was named CuBTC-NH_2-2.

2.3 *Photocatalytic experiments*

The synthesized MOFs were used as photocatalysts to degrade the organic dyes RB171 and AB1 in aqueous solution. An amount of 5 mg catalyst was added to 20 mL of dye solution (100 mg/L) followed by sonication in the dark for 5 min. The mixture was exposed to natural sunlight on a balcony for the degradation process. After 24 h, the mixture was separated by centrifugation, and the concentration of clear dye solution was determined by UV-visible spectrophotometry. Degradation experiments were performed continuously from April 8, 2019, to May 20, 2019 (irradiation site: 36.07°W and 120.4°N). The removal efficiency was calculated as the fraction of dye concentration after and before irradiation. The initial pH of the dye solution was adjusted by the addition of 0.1 M NaOH and 0.1 M HCl solutions.

2.4 *Characterization*

FT-IR spectra were recorded on a Thermo Nexus 470 FT-IR spectrometer (Nicolet) using KBr discs. The pore and surface properties were analyzed by nitrogen adsorption-desorption isotherms at -196 °C with an Autosorb-iQ-MP surface area and porosity analyzer (Quantachrome). The phases and structures of samples were investigated by XRD analysis with a D-MAX 2500/PC diffractometer (Rigaku).

3. Results and discussion

3.1 *Catalyst characterization*

FT-IR spectra of 1,3,5-H_3BTC and CuMOFs are displayed in Figure 2(a). The peaks between 1,680 and 1,730 cm^{-1} present in the spectrum of 1,3,5-H_3BTC disappeared after the reaction, indicating that all COOH groups in 1,3,5-H_3BTC were fully deprotonated. The double peaks at about 1,640/1,562 cm^{-1} could be attributed to the asymmetric stretching vibration of the -C = O group in -COO. In addition, the peaks at about 1,450/1,373 cm^{-1} were classified as symmetric stretching vibration peaks of the -C-O group.[26] The absorption bands of C-O-Cu were found at 1,112 and 1,045 cm^{-1}. The broad band at about 3,440 cm^{-1} possibly belonged to water in the micropores of MOFs. After modification by ethylene diamine, the observed characteristic amino absorption peaks at 3,401 cm^{-1} and 3,278 cm^{-1} were attributed to the stretching vibration of N-H in R-NH_2 and R-NH-Cu, respectively.[27,28] Furthermore, the N-H bending vibration in R-NH_2 was present at 1,562 cm^{-1}. The absorption peak at 1,157 cm^{-1} was assigned to the C-N stretching vibration.

The stretching vibration peaks at 2,975 cm^{-1} corresponded to the -CH_2CH_2- group in ethylene diamine. These results suggested that CuBTC-NH_2 was successfully prepared. Only one of the -NH_2 groups in $NH_2CH_2CH_2NH_2$ was involved in the reaction with CuBTC, and the other -NH_2 group remained an active primary amine.

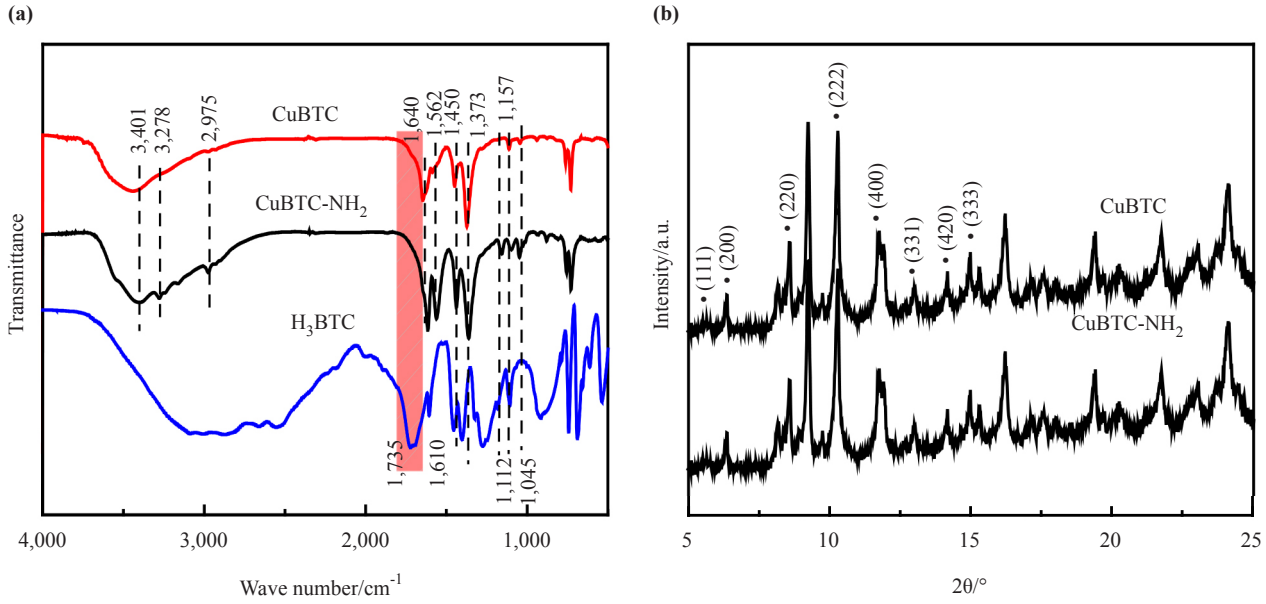

Figure 2. FT-IR spectra (a) and XRD patterns (b) of catalysts

Figure 2(b) shows the XRD patterns to confirm the phases and purities of Cu-BTC and Cu-BTC-NH_2. The peaks at the 2θ values 5.8°, 6.7°, 9.5°, 11.6°, 13.4°, 14.9°, 16.4°, and 17.5° corresponded to the crystal planes (111), (200), (220), (222), (400), (331), (420), and (333) of CuBTC, which was consistent with previous reports.[29] For CuBTC-NH_2, the 2θ peaks were similar to the data of CuBTC, indicating that the post-modification process did not change the crystal structure of CuBTC,[30] suggesting that ethylene diamine only substituted the water molecules in CuBTC and coordinated with copper atoms to form CuBTC-NH_2.

Nitrogen adsorption-desorption analysis based on the Brunauer-Emmett-Teller (BET) method was conducted on the synthesized MOFs at 77 K. The obtained pore parameters are listed in Table 2. While CuBTC exhibited large BET surfaces, the surface area of CuBTC-NH_2 significantly decreased and reduced further with increasing amounts of ethylene diamine. The mean pore diameter increased with the addition of ethylene diamine, which was attributed to the blocking of some pores in CuBTC by ethylene diamine.

Table 2. Pore parameters of the synthesized MOFs

MOFs	S_{BET}(m^2/g)	V(cm^3/g)	D(nm)
CuBTC	1016.745	0.522	2.547
CuBTC-NH_2	92.099	0.166	7.195
CuBTC-NH_2-2	19.784	0.064	27.670

3.2 *Catalytic activity*

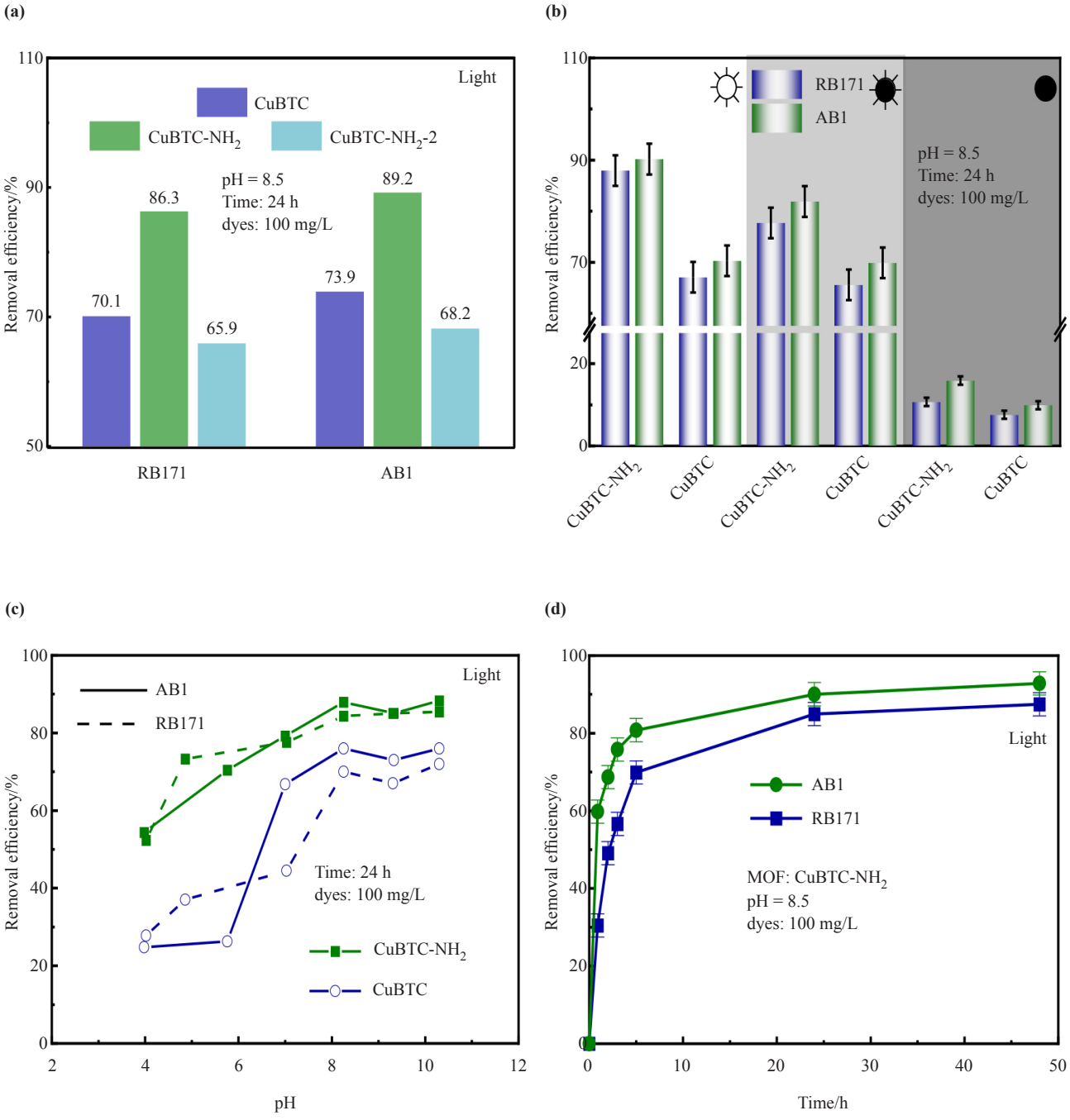

Figure 3. Removal efficiency of dyes by MOFs. (a) MOF structure, (b) light intensity, (c) initial pH of the dye solution, and (d) reaction time

Figure 3(a) shows the photocatalytic activity of the MOF catalysts for the oxidation and removal of two anionic dyes in solution under sunlight irradiation. Cu-BTC achieved a certain decolorization of the aqueous solution but only removed 70% of the two dyes. However, after the introduction of amino groups into the molecular structure of CuBTC, different catalytic activities were found for the obtained CuBTC-NH_2. The removal efficiencies of the dyes increased to approximately 90% in the presence of CuBTC-NH_2, which was much higher than the removal rate of 65% observed for

CuBTC-NH_2-2. The significant improvement in dye degradation by CuBTC-NH_2 could be attributed to the modification effect of amino groups in ethylene diamine. The amino groups in MOFs, as electron donors, effectively absorb visible light and improve the photocatalytic activities of MOFs.[21] According to previous reports, positive holes are generated on the aromatic ligands, while photo-ejected electrons are received by the metal nodes in both visible-light and UV-induced photocatalysis.[31,32] The photocatalytic performance of MOFs is attributed to the ligand-to-cluster charge transfer.[33,34] Dyes are degraded through the oxidation by holes on the aromatic ligands.[33] The long life of holes can favor the oxidation reaction. Amino groups in CuBTC-NH_2 could accept electrons, thereby inhibiting the recombination of holes and electrons and prolonging the life of holes.[35] However, an excessive amount of amino groups could sharply decrease the surface area of CuBTC-NH_2-2, resulting in a low adsorption rate between dyes and the MOF and low mass transfer of the reactant molecules.[18]

Table 3. Photodegradation of dyes using different MOFs in visible light or sunlight

Photocatalyst	Dye	Time	Dye Concentration	Removal Efficiency	Reference
		(h)	(mg /L)	(%)	
HKUST-1	Methyl Blue	1.5	10	53	40
NNU-36	Rhodamine B	1.17	100	46.6	41
Fe_3O_4@SiO_2@PCN-222(Fe)	Rhodamine B	2	100	92	42
	Erythrosine B	2	100	99	42
	Rose Bengal	2	100	98	42
ZIF-8/BiFeO	Rhodamine B	1.5	10	99	43
MIL-53(Fe)	Methylene blue	0.67	-	4	6
MIL-53(Al)/TiO_2	Methylene blue	4.0	12	95	44
MIL-53(Al)	Methylene blue	4.0	12	51	44
MIL-101(Fe)	Rhodamine B	5.0	10	87.4	18
ZnO/MIL-101(Fe)	Rhodamine B	5.0	10	97.1	18
NH_2-MIL-101(Fe)	Direct blue	19.0	20	65.7	21
CuBTC-NH_2	Reactive Blue 171	24	100	85	This work
CuBTC-NH_2	Acid Black 1	24	100	90	This work

Figure 3(b) shows the effect of light intensity on photocatalysis. In dark mode, the dyes were difficult to be removed by CuMOFs through the direct adsorption mechanism.[33] However, under sunlight conditions, the catalytic abilities of CuBTC and CuBTC-NH_2 caused a significant improvement in dye removal, which increased with increasing

irradiation. Positive holes generated from photoexcitation were the important driving force for the photocatalytic degradation of dyes under strong light.[36,37] In this work, too, strong light facilitated the removal of dyes under CuBTC-NH_2 catalysis. The presence of amino groups enhances the electron transfer capability, thereby enhancing the oxidation capacity of the catalyst towards dye molecules.[21,32]

The initial pH value of the dye solution changed the ionic states of dyes and influenced photodegradation, as shown in Figure 3(c). The removal efficiency of dyes increased with the increase in pH from 3.0 to 8.0 and then remained constant in basic solution. Cu-BTC-NH_2 catalyzed the photodegradation of dyes in a wider pH range, which is different from previous reports that metronidazole photodegradation using UiO-66-NH_2 was found to be more effective at low pH values (pH 2).[38] In acid or neutral solutions, CuBTC-NH_2 showed significantly higher catalytic degradation ability towards dyes compared to CuBTC. This difference decreased in basic solution. Under different pH conditions, different active species existed in the photocatalytic reaction system, leading to distinct driving forces for the oxidation of dye molecules. In acidic environments, the hole-electron effect was the major driving force for dye oxidation. Amino groups in CuBTC-NH_2 were more likely to form amino cation structures (-NH_3^+) under acidic conditions and inhibited efficiently the recombination of holes and electrons to enhance the oxidation of dye molecules by holes.[35] In basic solution, more OH^- could react with holes on the surface of MOFs to generate OH• radicals with strong oxidation capacity, which would promote the degradation of dyes.[18,39]

The effect of reaction time on the removal ratios of RB171 and AB1 is shown in Figure 3(d). Due to the low energy of visible light, the degradation process was slow.[36] After 1 h of sunshine irradiation, about 30-60% of RB171 and AB1 were removed. When the wastewater was exposed to sunlight for 24 h, 90% of the dyes degraded, which was consistent with previous literature.[31] Table 3 presents the comparison of degradation in visible light, indicating that CuBTC-NH_2 exhibited excellent catalytic properties.

3.3 *Regeneration of MOFs*

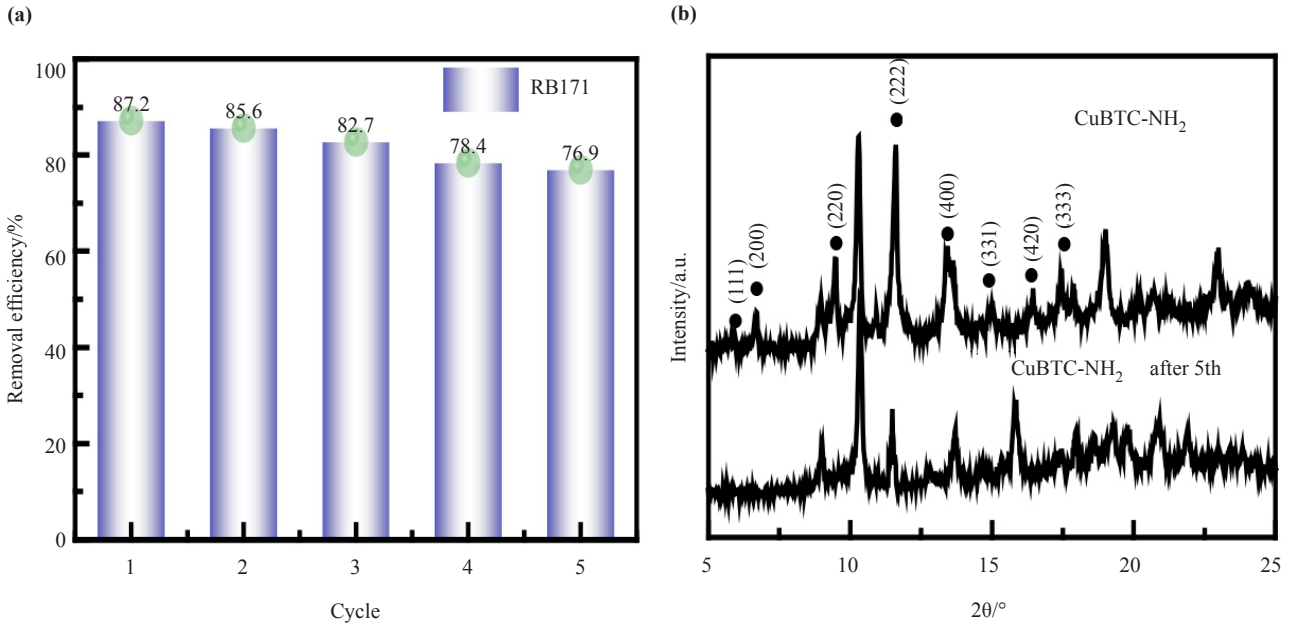

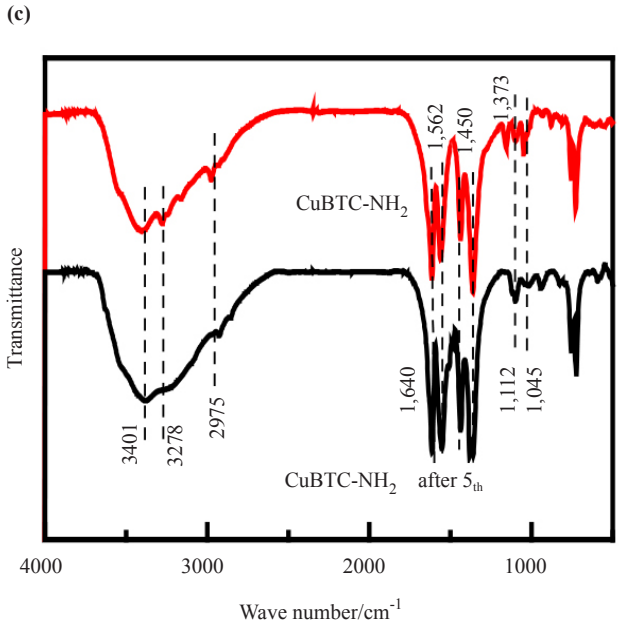

Figure 4. (a) Regeneration properties, (b) XRD patterns, and (c) FT-IR spectrum of CuBTC-NH_2 before and after dye degradation

The most challenging problem in efficient dye degradation is the regeneration of the photocatalyst. In the cycle experiment shown in Figure 4(a), the removal efficiency of RB171 decreased slightly from 87.2% to 76.9% after five cycles using CuBTC-NH_2 as photocatalyst. Approximately 10% decline in degradation over five cycles indicated the good stability of CuBTC-NH_2 in the reaction process. The XRD data in Figure 4(b) showed no significant changes before and after the degradation reaction, corroborating the good stability and regeneration ability of CuBTC-NH_2. The stability of ethylene diamine in MOFs was confirmed by the FT-IR data in Figure 4(c). The absorption bands related to -NH_2, -NH-, and -CH_2CH_3 were still observed after five cycles, indicating the excellent stability of CuBTC-NH_2. These data suggested that the observed decline in dye removal might be attributed to the blockage of pores in CuBTC-NH_2. Consequently, CuBTC-NH_2 has great potential as a photocatalyst for dye degradation under sunlight.

3.4 *Degradation mechanism*

The dyes used in the experiment were all azo dyes, containing -OH and -NH_2 groups in their molecular structure, as shown in Figure 1. According to Figures 5(a) and 5(b), there was a noticeable color change from blue to pink during the degradation process of the dye. In addition, the maximum absorption peaks of the dye shifted from 600-615 nm to about 520 nm in the visible region. Because AB1 and RB171 were diazo dyes, the blueshift of the absorption peaks indicated that the azo structures in the dye molecules were attacked. The weak absorption at 520 nm revealed that the dye molecules were not completely destroyed.[45] The lower intensity of the absorption peaks of the dye was consistent with the decrease in the decolorization rate of the dye solution. In the UV region, the new absorption peaks at 357-380 nm were attributed to smaller molecular degradation products.

Due to the reactivity differences between the two types of azo structures, characterized by ortho-hydroxyl and ortho-amino groups, the cleavage of the azo bond may occur in a certain sequence. To further determine the sequence of the azo bond breakdown, AB1 was separated into two monoazo dyes, named AB1-L and AB1-R.[46] Based on the UV-visible absorption data shown in Figure 5(c), the maximum absorption wavelength of AB1-R was observed at 523 nm, similar to the absorbance wavelengths of degraded AB1 and RB171 in the visible region. This indicated that the degradation process initially occurred at the AB1-L side, specifically targeting the azo bond in ortho-position of the amino group. The photocatalytic degradation of AB1-L was performed under the same condition and is shown in Figure 5(d). After 1 h of sunshine irradiation, about 60% of AB1-L were removed, which was similar to the degradation level

of AB1.[47,48] These results confirmed that the diazo group in ortho-position of the amino group in AB1 reacted first. After degradation, generated *p*-aniline derivatives with maximum absorption at 380 nm were the major products. Based on the above results, the possible degradation process of diazo dyes under CuBTC-NH_2 catalysis is provided in Figure 6.

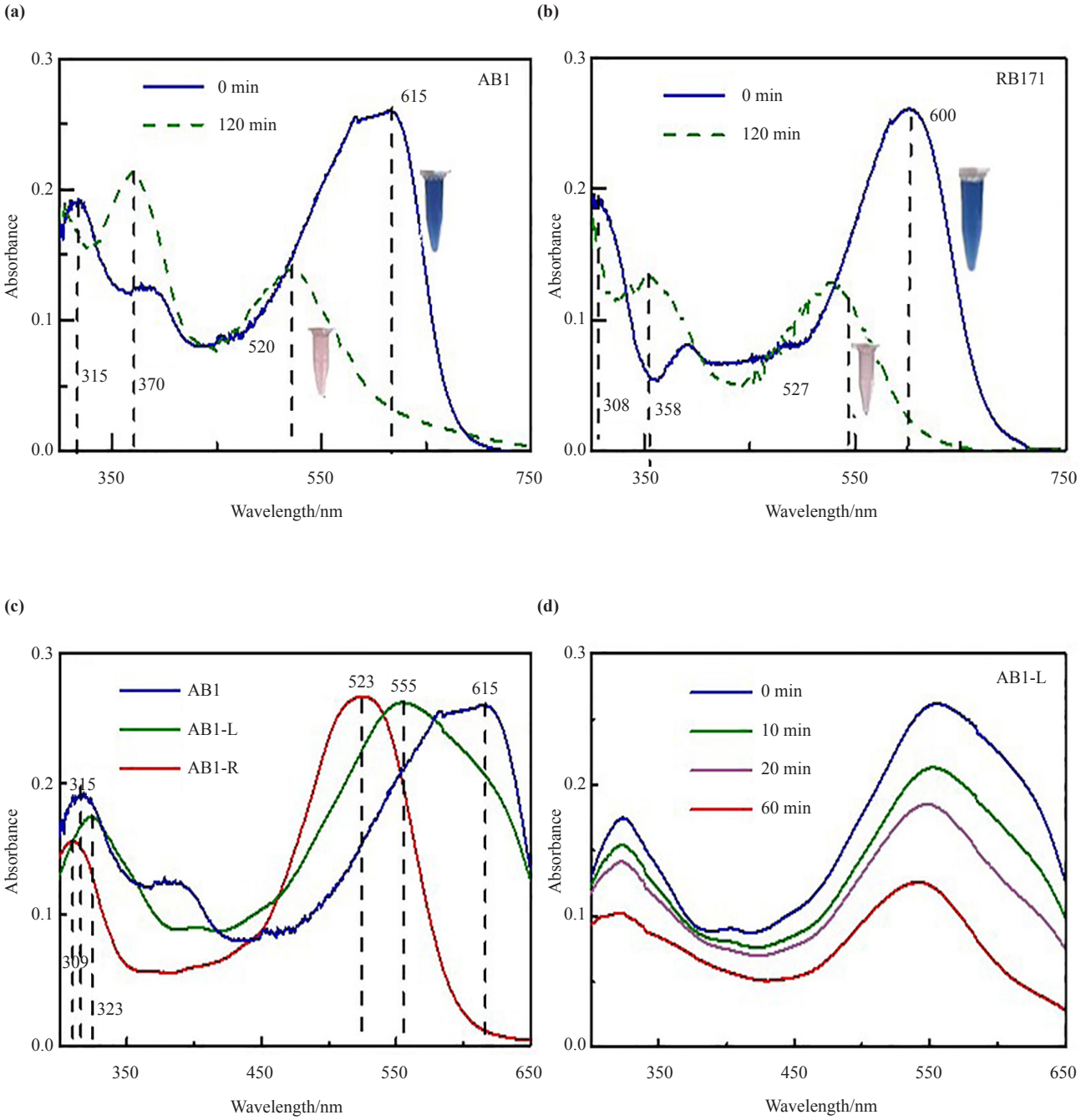

Figure 5. UV-visible absorption spectra of (a) AB1 and (b) RB171 before and after degradation and of (c) dye intermediate and (d) AB1-L degradation

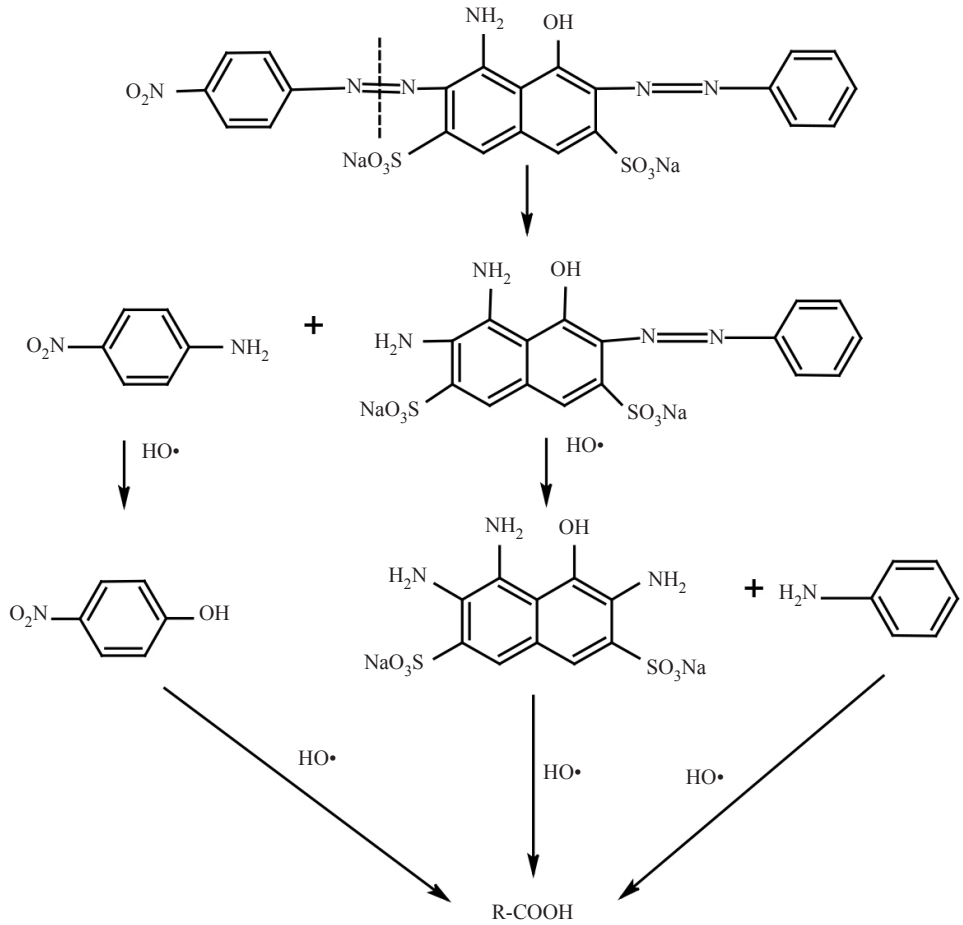

Figure 6. Degradation mechanism of AB1

4. Conclusion

Ethylene diamine, as an amine group provider, was used to synthesize CuBTC-NH_2 by a post-modification method. The prepared CuMOFs were used as photocatalysts to degrade dye wastewater under sunlight irradiation. Batch catalytic experiments indicated that the addition of ethylene diamine to CuBTC enhanced the photocatalytic activity of the obtained CuBTC-NH_2 catalyst. 90% of the dyes were removed within 24 h of exposure to sunlight. Furthermore, weakly basic conditions favored the degradation process of the dye wastewater. CuBTC-NH_2 demonstrated excellent regeneration and reuse capability over at least five cycles. These results provide insights into the removal of dyes using NH_2-modified MOF as a novel photocatalyst under visible-light irradiation.

Acknowledgments

The authors wish to acknowledge the financial support provided by the Innovation improvement project of technological small and medium-sized enterprises in Shandong Province (No 2021TSGC1360), National Natural Science Foundation of Shandong Province (No ZR2017MB024).

Conflict of interest

The authors declare no competing financial interest.

References

[1] Lebkiri, I.; Abbou, B.; Hsissou, R.; Safi, Z.; Sadiku, M.; Berisha, A.; El Amri, A.; Essaadaoui, Y.; Kadiri, L.; Lebkiri, A.; Rifi, E. H. *J. Mol. Liq*. **2023,** *372*, 121220.
[2] Kadiri, L.; Ouass, A.; Hsissou, R.; Safi, Z.; Wazzan, N.; Essaadaoui, Y.; Lebkiri, I.; El Khattabi, O.; Housseine Rifi, E.; Lebkiri, A. *J. Mol. Liq.* **2021,** *343*, 116971.
[3] Al Degs, Y. S.; El Barghouthi, M. I.; Khraisheh, M. A.; Ahmad, M. N.; Allen, S. J. *Sep. Sci. Technol.* **2005,** *39*, 97-111.
[4] El Amri, A.; Kadiri, L.; Hsissou, R.; Lebkiri, A.; Wardighi, Z.; Rifi, E. H.; Lebkiri, A. *J. Mol. Struct.* **2023,** *1272*, 134098.
[5] Bensalah, J.; Idrissi, A.; Faydy, M. E.; Doumane, G.; Staoui, A.; Hsissou, R.; Lebkiri, A.; Habsaoui, A.; Abdelkader, Z.; Rifi, E. H. *J. Mol. Struct.* **2023,** *1278*, 134849.
[6] Uddin, M. J.; Ampiaw, R. E.; Lee, W. *Chemosphere* **2021,** *284*, 131314.
[7] Jebli, A.; Amri, A. E.; Hsissou, R.; Lebkiri, A.; Zarrik, B.; Bouhassane, F. Z.; Hbaiz, E.; Rifi, E. H.; Lebkiri, A. *J. Taiwan. Inst. Chem. Eng.* **2023,** *149*, 105006.
[8] Patil, N. N.; Shukla, S. R. *Environ. Prog. Sustainable Energy* **2015,** *34*, 1652-1661.
[9] Gupta, V. K.; Suhas. *J. Environ. Manage.* **2009,** *90*, 2313-2342.
[10] Iraqui, S.; Dubey, A.; Savarimuthu, I.; Shankar, A.; Jaiswal, A.; Bahadur, I.; Uddin, I.; Mohammad, F. *J. Mol. Liq.* **2023,** *388*, 122794.
[11] Uddin, I. *J. Photochem. Photobiol. A* **2021,** *421*, 113512.
[12] Gupta, V. K.; Jain, R.; Agarwal, S.; Nayak, A.; Shrivastava, M. *J. Colloid Interface Sci.* **2012,** *366*, 135-140.
[13] Du, J. J.; Yuan, Y. P.; Sun, J. X.; Peng, F. M.; Jiang, X.; Qiu, L. G.; Xie, A. J.; Shen, Y. H.; Zhu, J. F. *J. Hazard. Mater.* **2011**, *190*, 945-951.
[14] Wan, Z.; Hu, X.; Li, C.; Zhang, J.; Wang, Q.; Fang, L.; Zhang, L.; Guo, Q.; Sun, D. *J. Environ. Chem. Eng.* **2023,** *11*, 109417.
[15] Llabrés i Xamena, F. X.; Corma, A.; Garcia, H. *J. Phys. Chem. C* **2007,** *111*, 80-85.
[16] Li, H.; Eddaoudi, M.; O'Keeffe, M.; Yaghi, O. M. *Nature* **1999,** *402*, 276-279.
[17] Fu, Y.; Sun, D.; Chen, Y.; Huang, R.; Ding, Z.; Fu, X.; Li, Z. *Angew. Chem. Int. Ed.* **2012,** *51*, 3364-3367.
[18] Amdeha, E.; Mohamed, R. S. *Environ. Technol.* **2021,** *42*, 842-859.
[19] Wang, D.; Jia, F.; Wang, H.; Chen, F.; Fang, Y.; Dong, W.; Zeng, G.; Li, X.; Yang, Q.; Yuan, X. *J. Colloid Interface Sci.* **2018,** *519*, 273-284.
[20] Liang, R.; Shen, L.; Jing, F.; Wu, W.; Qin, N.; Lin, R.; Wu, L. *Appl. Catal. B* **2015,** *162*, 245-251.
[21] Li, X.; Wang, Y.; Guo, Q. *Heliyon* **2022,** *8*, e09942.
[22] Cao, Y.; Wang, G.; Liu, H.; Li, Y.; Jin, Z.; Ma, Q. *Int. J. Hydrog. Energy* **2021,** *46*, 7230-7240.
[23] Quan, Y.; Wang, G.; Jin, Z. *ACS Appl. Energy Mater.* **2021,** *4*, 8550-8562.
[24] Schlichte, K.; Kratzke, T.; Kaskel, S. *Microporous Mesoporous Mater.* **2004,** *73*, 81-88.
[25] Hwang, Y. K.; Hong, D. Y.; Chang, J. S.; Jhung, S. H.; Seo, Y. K.; Kim, J.; Vimont, A.; Daturi, M.; Serre, C.; Férey, G. *Angew. Chem. Int. Ed.* **2008,** *47*, 4144-4148.
[26] Pu, F.; Liu, X.; Xu, B.; Ren, J.; Qu, X. *Chem. Eur. J.* **2012,** *18*, 4322-4328.
[27] Silambarasan, A.; Kavitha, H. P.; Ponnusamy, S.; Navaneethan, M.; Hayakawa, Y. *Appl Catal a Gen.* **2014,** *476*, 1-8.
[28] Xu, Q.; Sun, D.; Qi, Y.; Duan, L. *Chem Eng Technol.* **2019,** *42*, 1070-1077.
[29] Lin, S.; Song, Z.; Che, G.; Ren, A.; Li, P.; Liu, C.; Zhang, J. *Microporous Mesoporous Mater.* **2014,** *193*, 27-34.
[30] Fu, Y.; Zhang, K.; Zhang, Y.; Cong, Y.; Wang, Q. *Chem. Eng. J.* **2021,** *412*, 128722.
[31] Kozlova, E. A.; Panchenko, V. N.; Hasan, Z.; Khan, N. A.; Timofeeva, M. N.; Jhung, S. H. *Catal. Today* **2016,** *266*, 136-143.
[32] Miguel, M.; Ragon, F.; Devic, T.; Serre, C.; Horcajada, P.; García, H. *Chemphyschem* **2012,** *13*, 3651-3654.
[33] Sadeghian, S.; Pourfakhar, H.; Baghdadi, M.; Aminzadeh, B. *Chemosphere* **2021,** *268*, 129365.
[34] Pattappan, D.; Kavya, K. V.; Vargheese, S.; Kumar, R. T. R.; Haldorai, Y. *Chemosphere* **2022,** *286*, 131875.
[35] Haque, E.; Lee, J. E.; Jang, I. T.; Hwang, Y. K.; Chang, J.-S.; Jegal, J.; Jhung, S. H. *J. Hazard. Mater.* **2010,** *181*,

535-542.
[36] Saeed, M.; Muneer, M.; Haq, A. U.; Akram, N. *Environ. Sci. Pollut. Res.* **2022,** *29*, 293-311.
[37] Guo, K.; Hussain, I.; Jie, G.; Fu, Y.; Zhang, F.; Zhu, W. *J. Environ. Sci.* **2023,** *125*, 290-308.
[38] Wang, Y. L.; Gómez Avilés, A.; Zhang, S.; Rodriguez, J. J.; Bedia, J.; Belver, C. *J. Environ. Chem. Eng.* **2023,** *11*, 109744.
[39] Adeel, M.; Saeed, M.; Khan, I.; Muneer, M.; Akram, N. *ACS Omega.* **2021,** *6*, 1426-1435.
[40] Zhang, J.; Su, C.; Xie, X.; Liu, P.; Huq, M. E. *RSC Adv.* **2020,** *10*, 37028-37034.
[41] Zhao, H.; Xia, Q.; Xing, H.; Chen, D.; Wang, H. *ACS Sustainable Chem. Eng.* **2017,** *5*, 4449-4456.
[42] Hariri, R.; Dehghanpour, S. *J. Phys. Chem. Solids* **2021,** *155*, 110126.
[43] Bethi, B.; Radhika, G. B.; Thang, L. M.; Sonawane, S. H.; Boczkaj, G. *Environ. Sci. Pollut. Res.* **2023,** *30*, 25532-25545.
[44] Zokaee, Z.; Mahmoodi, N. M.; Rahimpour, M. R.; Shariati, A. *J. Solid State Chem.* **2022,** *307*, 122747.
[45] Chen, B. Y. *Process Biochem.* **2002,** *38*, 437-446.
[46] Reutergådh, L. B.; Iangphasuk, M. *Chemosphere* **1997,** *35*, 585-596.
[47] Meetani, M. A.; Hisaindee, S. M.; Abdullah, F.; Ashraf, S. S.; Rauf, M. A. *Chemosphere* **2010,** *80*, 422-427.
[48] Ball, M. T.; Hay, J.; Masrouji, H. M.; Sugden, J. K. *Dyes Pigm.* **1992,** *19*, 51-57.